Scientia Iranica A (2022) 29(3), 1038–1058

Sharif University of Technology
Scientia Iranica
Transactions A: Civil Engineering
http://scientiairanica.sharif.edu

Effectiveness of a vertical micropile system in mitigating the liquefaction-induced lateral spreading effects on pile foundations: 1 g large-scale shake table tests

A. Kavand[a,*], S.M. Haeri[b], J. Raisianzadeh[a,1], and S. Afzalsoltani[b]

a. *School of Civil Engineering, College of Engineering, University of Tehran, Tehran, Iran.*
b. *Department of Civil Engineering, Sharif University of Technology, Tehran, Iran.*

Received 4 September 2020; received in revised form 19 July 2021; accepted 25 October 2021

KEYWORDS
Micropile;
Liquefaction;
Lateral spreading;
Shake table test;
Pile group;
Remedial measure.

Abstract. Liquefaction-induced lateral spreading caused severe damages to pile foundations during past earthquakes. Micropiles can be used as a mitigation strategy against lateral spreading effects on pile foundations. However, the available knowledge about the possible efficiency of this strategy is quite limited. In this regard, the present study aims to evaluate the effectiveness of a vertical micropile system as a lateral spreading countermeasure using large-scale 1 g shake table tests on 3 × 3 pile groups. The results showed that the micropile system was not able to effectively reduce the bending moments in piles; however, it considerably reduced the lateral soil pressures exerted on the upslope piles of the group by the upper non-liquefiable layer. The employed micropiles restricted the lateral displacement of the upper non-liquefiable layer and, partially, that of the liquefiable layer, especially at upper depths. Several solutions were offered to enhance their performance including increasing the number of micropiles with a tighter pattern and using stiffer micropiles or fixing them in the underlying non-liquefiable layer.

1. Introduction

The ground instability associated with liquefaction is a major threat to pile-supported structures. Many of these structures were severely damaged by this type of ground instability during past earthquakes. These reported damages were more extensive in areas with mildly-sloped grounds or waterfront areas with lateral spreading. For instance, several destructive cases were caused by the following earthquakes: the 1964 Niigata, Japan; the 1989 Loma Prieta, USA; the 1995 Kobe, Japan; the 2010 Haiti; and the 2011 Tohoku earthquakes [1–7]. Liquefaction-induced lateral spreading usually occurs in mildly-sloped grounds or areas ending in a free face as a result of liquefaction in saturated loose granular soils. The excess pore water pressures developed during earthquakes can significantly decrease the shear strength of such soils, hence their lateral movement towards downslope or free face due to the static shear stresses [8]. Horizontal displacements caused by lateral spreading can be as long as several meters, thus exerting extra lateral pressure on the pile foundations subjected to it. The response of

1. *Present address: Department of Civil Engineering, Pardis Branch, Islamic Azad University, Pardis, Iran.*
*. *Corresponding author. Tel.: +98 21 66462616; Fax: +98 21 66403808*
E-mail address: akavand@ut.ac.ir (A. Kavand)

doi:10.24200/sci.2021.56729.4876

pile foundations in laterally spreading ground has been extensively investigated by numerous researchers through 1 g shake table tests [9–16], Ng centrifuge tests [17–22], or field experiments [23]. In addition, different experimental studies have been conducted on retrofit strategies for prevention or mitigation of lateral spreading damages to the existing pile foundations. In general, a wide variety of potential mitigation measures can be adopted to overcome the lateral spreading effects. These mitigation measures including soil stabilization or densification are employed to completely or partially prevent liquefaction and consequently lateral spreading [24–33], restriction of ground displacement using appropriate underground barriers [34–36], different ground improvement procedures including jet grouting, deep soil mixing using stone columns [37–41], or insertion of micropiles. Among all these mitigation methods, use of micropiles is a practical option for rehabilitation of the existing pile foundations in liquefiable soils particularly in sites characterized by some construction constraints such as low head-room, restricted access, and noise and vibration restrictions. A micropile is a small-diameter, drilled, and grouted non-displacement pile which is reinforced by a steel bar [42].

Numerous studies have been conducted on the behavior of micropiles under static loading. In recent years, a number of studies have also evaluated the performance of micropiles under seismic loading through physical modeling [43–45] or field tests [46–49]; however, the performance of micropiles in liquefiable grounds has not been adequately investigated yet [50–54]. This limited body of research is briefly reviewed herein. McManus et al. [50] conducted shake table experiments on loose sand to study the effectiveness of the inclined micropiles in preventing liquefaction on level grounds. Given that the sand tested in these experiments was dry, they used the amplitude of cyclic shear strain in the dry soil as an index of liquefaction potential. They also argued that if the sand particles were small enough, liquefaction would not happen in saturated conditions. Although their model used dry sand, they concluded that the adopted reinforcement system could probably prevent liquefaction in saturated sand, as well. Shahrour and Juran [51] conducted centrifuge experiments to examine the effectiveness of vertical and inclined micropiles as the stiffening elements in restraining soil movement. They found that liquefaction was prevented in the area treated by micropiles since these micropiles decreased the generation of excess pore water pressures by restraining the ground movements. Mitrani and Madabhushi [52] performed a number of centrifuge experiments to explore the effectiveness of inclined micropiles inserted outside the footprint of an existing building as a liquefaction remediation method. They reported a reduction in building settlements when applying a relatively small intensity shaking and argued that the depth of liquefaction occurrence was above the bottom of the uppermost micropile. Further, they implied that direct insertion of micropiles under the structure and through the whole depth of liquefiable layer could improve their effectiveness. GuhaRay et al. [53] evaluated the performance of micropiles around a structure through small-scale shake table tests. They tested a different spacing-to-diameter ratio of micropiles and applied shaking with different amplitudes on each model until the model was fully liquefied. They found that using micropiles with an appropriate spacing-to-diameter ratio could increase soil resistance as well as the number of loading cycles required for liquefaction initiation. Farhangi et al. [54] examined the effectiveness of micropiles in reducing the liquefaction risk using in-situ tests. The simplified liquefaction analyses based on the results from SPT and CPT tests indicated that micropiles could effectively reduce the liquefaction risk. The micropiles used in this case study were installed based on the post-grouting technique [42], which caused penetration of grout into the nearby soil, hence improvement of soil properties.

The interaction among the micropiles, liquefied ground, and existing piles has not been investigated in previous studies, and most of these studies have been conducted in level ground. In this respect, the present study aims to evaluate the performance of vertical micropiles in remediation of the destructive impacts of liquefaction-induced lateral spreading on the existing pile groups based on large-scale 1 g shake table tests. The interactions among micropiles, liquefied ground, and pile group can be studied better using large-scale physical models, which have rarely been used in previous studies. In this research, two densely instrumented large-scale physical models were built and tested using a 1 g shaking table. The first model (thereafter termed as Model A) was established with no mitigation measure while the second one (thereafter termed as Model B) included vertical micropiles. The most important findings of the conducted experiments are discussed in the following parts.

2. Physical models

This study was conducted at the Earthquake Engineering Research Center (EERC) at Sharif University of Technology (SUT). This research center maintains the SUT shake table that consists of a 4 m $\times$ 4 m deck with three degrees of freedom capable of carrying payloads up to 300 kN. This 1 g shake table is powered by a longitudinal actuator with a capacity of 500 kN and two transversal actuators with a capacity of 2×200 kN. The maximum strokes of actuators are ±125 and ±200 mm in the longitudinal and transversal directions, respectively. The actuators can provide a maximum horizontal acceleration of 20 m/s^2 with a broad range of frequencies from 0.01 Hz to 50 Hz in both directions.

The model container used in this study is 3.5 m long, 1.0 m wide, and 1.5 m high. This box is long enough to facilitate the free movement of the soil downslope during lateral spreading. Two watertight windows covered with Plexiglas were built on one side of the box to monitor the lateral movement of model ground during the tests.

2.1. Scale similitude law

Selection of the appropriate scaling law is an indispensable part of physical modeling. In this regard, the present study employed the scale similitude relationships proposed by Iai [55] and Iai et al. [56]. The scaling factors of the key model parameters are outlined in Table 1. As observed, a geometrical scaling factor of $\lambda = 8.0$ was selected, considering the dimensions of the shaking table deck and the model container. More details about the application of scaling factors to different physical model elements are given in the following sections.

2.2. Ground layers

The ground considered on the prototype scale resembles the typical conditions of the liquefied sites during past earthquakes. The prototype ground is composed of three layers including an upper non-liquefiable layer, a middle sandy liquefiable layer with a relative density of about 40%, and a non-liquefiable dense base layer. The properties of each layer are listed in Figure 1. According to this figure, the slope of all ground layers was 7% in the longitudinal direction, indicating the mildly-sloped grounds prone to lateral spreading.

The soil used for model ground construction is standard Firoozkuh silica sand (No. 161) which is crushed sand with angular particles in golden yellow. Due to its uniform gradation curve, Firoozkuh sand is commonly used as a standard sand in the study of liquefaction in Iran. Table 2 summarizes the index geotechnical properties of Firoozkuh sand.

Table 1. Scaling factors for 1 g shaking table tests.

Parameter	Scaling factors (prototype/model)	Scaling factors in this study (prototype/model)
Length (l)	λ	8.0
Density (ρ)	λ_ρ	1.0
Strain (ε)	λ_ε	1.0
Time (t)	$(\lambda\lambda_\varepsilon)^{0.5}$	2.828
Frequency (f)	$(\lambda\lambda_\varepsilon)^{-0.5}$	0.353
Acceleration ($\ddot{u}$)	1.0	1.0
Displacement (u)	$\lambda\lambda_\varepsilon$	8.0
Stress (σ)	$\lambda\lambda_\rho$	8.0
EI of pile	$\lambda^5\lambda_\rho/\lambda_\varepsilon$	32768
Bending moment	$\lambda^4\lambda_\rho$	4096

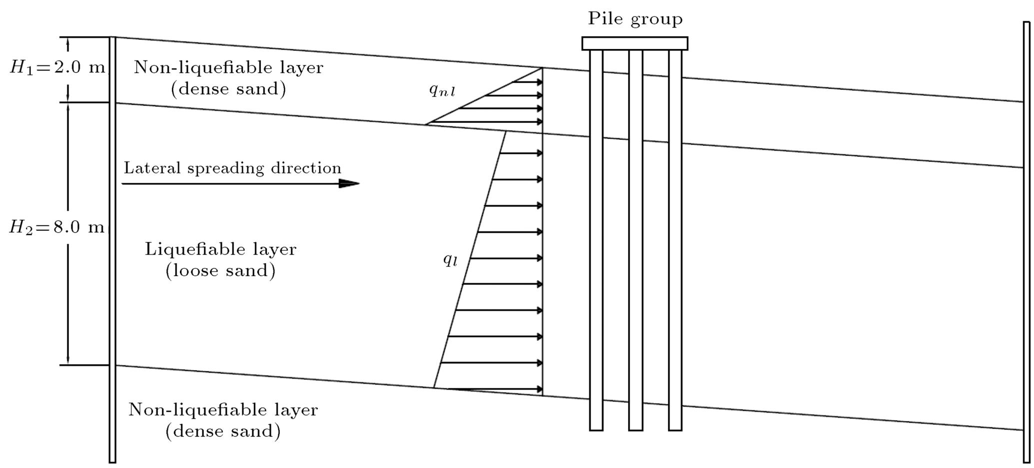

Figure 1. Schematic view of the ground layers and pile groups on the prototype scale along with the lateral earth pressures exerted on the piles based on Japan Road Association (JRA) code [58].

Table 2. Index properties of Firoozkuh silica sand (No. 161).

Specific gravity	Maximum void ratio ($e_{\max}$)	Minimum void ratio ($e_{\min}$)	Coefficient of uniformity (C_u)	Mean grain size (D_{50}) (mm)	D_{10} (mm)	D_{90} (mm)	Friction angle* (deg)	Cohesion (kPa)
2.698	0.87	0.608	1.49	0.24	0.18	0.39	32	0

* for $D_r = 15\%$

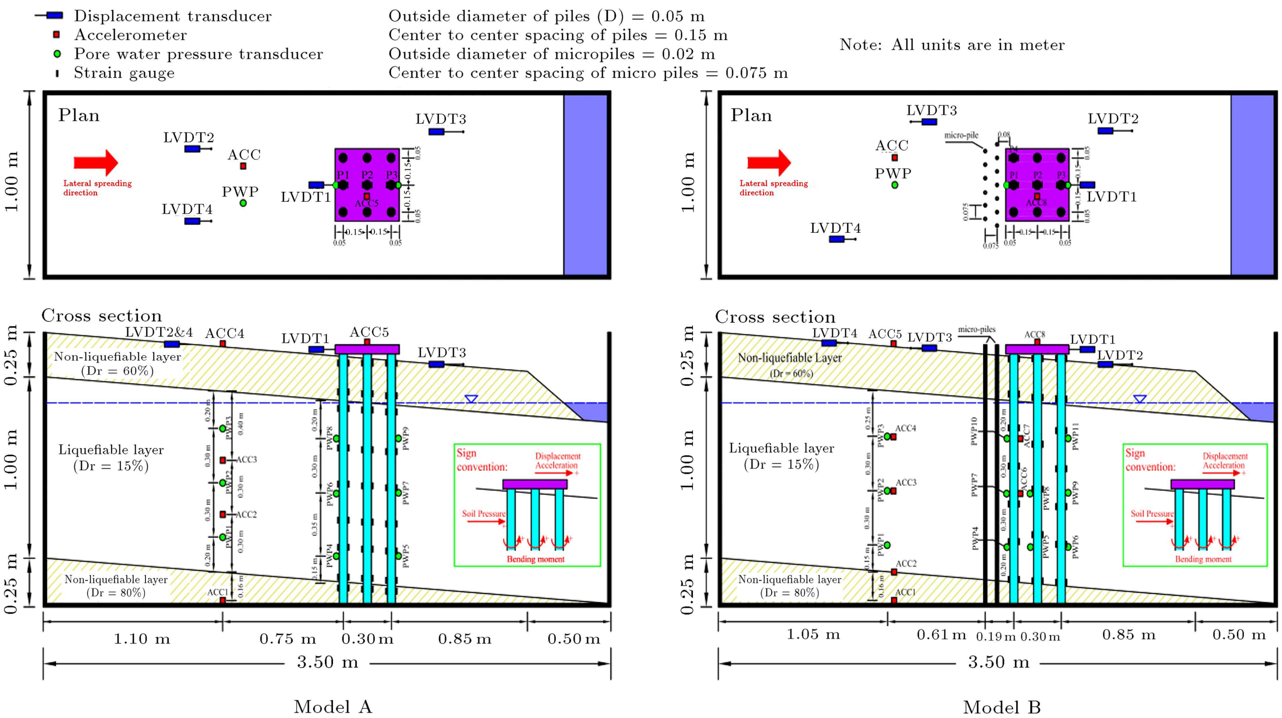

Figure 2. Plan view and cross-section of the physical models along with the instrumentation layout.

Considerable attention has been drawn to reproducing the contractive behavior of loose sand during liquefaction. To this end, the sandy liquefiable layer of the physical model was constructed looser than the prototype to compensate for the effects of the reduced overburden pressure in the scaled model, which caused dilative behavior and even prevented liquefaction. To this end, the concept of brittleness index proposed by Vargas-Monge [57] was employed. The brittleness index obtained by the peak and residual strength of the soil should have the same value, both in the model and prototype. In this respect, the relative density of the liquefiable layer should be reduced from 40% on the prototype scale to about 15% on the model scale to keep the brittleness index constant. The relative densities of the upper and lower non-liquefiable layers on the model scale were also assumed to be about 60% and 80%, respectively. Since the liquefiable layer of the models was looser than that of the prototype, type III of the scaling factors proposed by Iai et al. [56] was implemented here.

As mentioned in Section 1, two physical models were established and tested in this research: one with no mitigation measure (Model A) and the other with vertical micropiles as a remediation strategy (Model B). Figure 2 shows the details of these models. The ground in both models is composed of three soil layers, as noted earlier. Thickness of each layer was calculated based on the geometric scaling factor. To achieve the relative density of 15%, the 1.0 m thick liquefiable layer was created through controlled deposition of sand in water from nearly zero height with a calibrated pluviator, as shown in Figure 3(b). The pluviator had a large bucket attached to three successive sieves and a perforated plate at the base [14]. The bottom and upper non-liquefiable layers were created using wet tamping technique and air pluviation method, respectively.

Of note, prior to construction of soil layers, the model piles were installed in the model box. All model piles were fixed at the bottom of the box in translational and rotational directions, and they were tightly inserted into the holes of a cap at the top. Before constructing the upper non-liquefiable layer, the micropiles in Model B were inserted in the liquefiable and bottom non-liquefiable layers.

Table 3. Design parameters of a 3 × 3 pile group on the prototype scale.

Parameter	Value
Thickness of the non-liquefiable layer (H_1)	2 m
Thickness of the liquefiable layer (H_2)	8 m
Unit weight of the non-liquefiable layer (γ_1)	18 kN/m^3
Unit weight of the liquefiable layer (γ_2)	20 kN/m^3
Internal friction angle of the non-liquefiable layer (φ)	30°
coefficient of passive lateral earth pressure (K_p)	3.0
Diameter of the prototype piles (D)	40 cm
$M_{\max} = \left[\frac{1}{2}K_p\gamma_1 H_1^2 \times \left(\frac{H_1}{3}+H_2\right) + 0.3\left(\gamma_1 H_1 H_2 \times \frac{H_2}{2} + 0.5\gamma_2 H_2^2 \times \frac{H_2}{3}\right)\right] \times 7D/9$	558.0 kN.m
$V_{\max} = \left[\frac{1}{2}K_p\gamma_1 H_1^2 + 0.3\left(\gamma_1 H_1 H_2 + 0.5\gamma_2 H_2^2\right)\right] \times 7D/9$	120.2 kN
28-day compressive strength of concrete (f'_c)	24 MPa
Elastic modulus of concrete (E_c)	23025 MPa

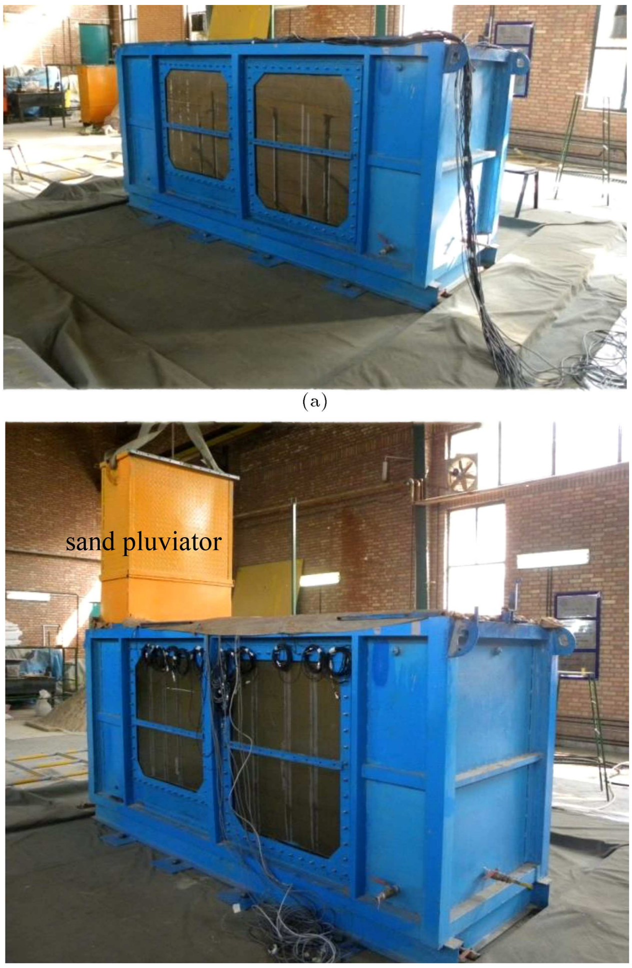

(a)

(b)

Figure 3. Side views of the physical models on the SUT shake table: (a) Model A and (b) Model B during construction of liquefiable layer.

2.3. Piles

The piles on the prototype scale were assumed to be Reinforced Concrete (RC) piles designed based on the regulations of Japan Road Association (JRA) code [58] to resist the lateral pressures resulting from lateral spreading. The lateral pressures applied to the pile group during lateral spreading (Figure 1) can be calculated as follows:

$$q_{nl} = C_{nl} K_P \gamma_{nl} h, \tag{1}$$

$$q_l = 0.3\left[\gamma_{nl} H_{nl} + \gamma_l \left(h + H_{nl}\right)\right]. \tag{2}$$

In Eq. (1), q_{nl} is the lateral pressure exerted on the non-liquefiable layer, C_{nl} a constant factor in the range of $0-1$, K_P the coefficient of the passive lateral earth pressure of the non-liquefiable layer, γ_{nl} the unit weight of the non-liquefiable overlying layer and h the depth from the free ground surface. In Eq. (2), q_l is the lateral pressure exerted by the liquefiable layer, H_{nl} the thickness of the upper non-liquefiable layer, and γ_l the unit weight of the liquefiable layer. The center-to-center spacing between the piles was three times the pile diameter. Table 3 summarizes the details of the design parameters of the 3 × 3 pile group.

The mechanical and geometrical characteristics of the piles on the model scale were subsequently calculated using the governing scale similitude relationships. More details of the geometrical and mechanical properties of the model piles are summarized in Table 4. The current study puts greater focus on the kinematic interaction between the piles and liquefied soil during lateral spreading rather than their dynamic interaction, mainly because the liquefaction-induced lateral spreading is somewhat a post-earthquake phenomenon in reality. In such a kinematic interaction, proper scaling of flexural stiffness of piles (EI) is of high significance. The model piles were made of High Density Polyethylene (HDPE) pipes. HDPE is the only available material in the market that can provide the required modulus of elasticity on the model scale according to EI scale factor in Table 1 while keeping the geometrical scaling factor satisfied. This study also focused on the kinematic forces caused by lateral spreading, and the inertial forces caused by the super-

Table 4. Geometrical and mechanical characteristics of the prototype and model piles.

Parameters according to the similitude law			
Parameter	**Scaling factor**	**Prototype**	**Model**
EI (kN.m^2)	$\lambda^5 = 8^5$	10826	0.33
Outer diameter (cm)	$\lambda = 8$	40	5.0
Values used for the model piles			
Outer diameter (cm)			5.00
Thickness (cm)			0.23
Inner diameter (cm)			4.54
I_{model} (cm^4)			9.83
E_{HDPE} (MPa)			1795
EI_{model} (kN.m^2)			0.18

structure were ignored. Therefore, the superstructure was not considered in the tests.

2.4. Micropiles

The prototype concrete micropiles were 15 cm in diameter, each of which was reinforced by the steel rebar number 28. The specifications of micropiles on the model scale were obtained based on the scale similitude relationships, as summarized in Table 5. Polypropylene pipes were used as the model micropiles that were inserted into the liquefiable as well as the bottom non-liquefiable layers followed by constructing the physical model with a spacing of 7.5 cm (center to center), as given in Figure 2.

2.5. Input motion

The shaking was applied to the model parallel to the direction of the sloping ground. It is a sinusoidal motion with an amplitude of 0.3 g and duration of 12.0 sec that comprises two short rising and falling ramps at the beginning and end. The shaking resembles an earthquake with a duration of about 34.0 sec on the prototype scale based on the time scaling factor. The frequency of shaking is 3.0 Hz, indicating an earthquake record in soft soil with a predominant period of about 1.0 sec on the prototype scale. More details about the specifications of the input motion are presented in Table 6. Of note, the scaling factor of the acceleration is equal to unity in 1 g model tests.

Table 5. Geometrical and mechanical characteristics of the prototype and model micropiles.

Parameters according to the similitude law			
Parameter	**Scaling factor**	**Prototype**	**Model**
EI (kN.m^2)	$\lambda^5 = 8^5$	214	0.007
Outer diameter (cm)	$\lambda = 8$	15	2.0
Values used for the model micropiles			
Outer diameter (cm)			2.00
Thickness (cm)			0.42
Inner diameter (cm)			1.16
I_{model} (cm^4)			0.68
$E_{Polypropylene}$ (MPa)			1000
EI_{model} (kN.m^2)			0.007

Table 6. Specifications of the input motion.

Parameter	**Scaling factor**	**Prototype**	**Model**
Peak ground acceleration (PGA)	1.0	0.3 g	0.3 g
Duration	$\lambda^{0.5} = 8^{0.5}$	34 sec	12 sec
Frequency	$\lambda^{-0.5} = 8^{-0.5}$	1.0 Hz	3.0 Hz

2.6. Instrumentation

As shown in Figure 2, to monitor the behavior of the physical models during shaking, different types of sensors were mounted at different locations of the models including the miniature pore pressure transducers in soil far from the piles (i.e., free field) and adjacent to the piles, accelerometers in the free field soil, and pile caps and displacement transducers on the ground surface as well as the pile caps. Moreover, according to this figure, several strain gauges were attached to different model piles in different locations to precisely measure their induced bending moments. The sign convention used for interpreting the measured parameters is shown in Figure 2. Figure 3 depicts two photographs of the physical models on the shake table deck (before the tests).

3. Acceleration records

A number of accelerometers were mounted on the free field soil to record the accelerations during lateral spreading (Figure 2). The recorded acceleration time histories for two tested models are presented in Figures 4 and 5, where the positive amplitude corresponds to the downslope direction. According to the general trend of the acceleration time histories, the free field soils in both models lost their shear strength within the initial few cycles of shaking leading to liquefaction. In both models, the ground surface accelerations exhibited some minor amplification relative to those at deeper depths due to the presence of the upper non-liquefiable layer. The spikes observed in the ground surface accelerations in the negative direction resulted from the successive return of the pile group towards upslope during shaking. In fact, the piles struck the upper non-liquefiable layer during each return of the pile group to the upslope, thus leading to the subsequent spikes in ground surface accelerations.

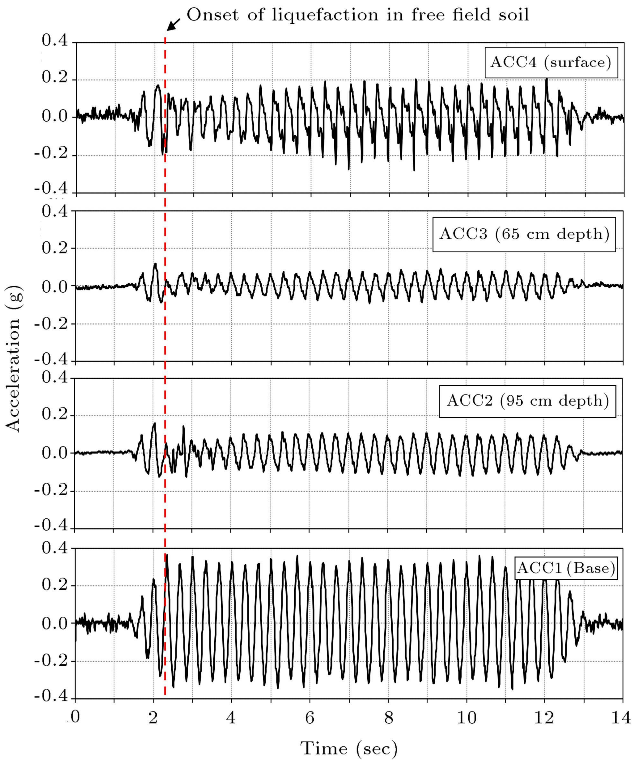

Figure 4. Time histories of acceleration in the free field soil (Model A).

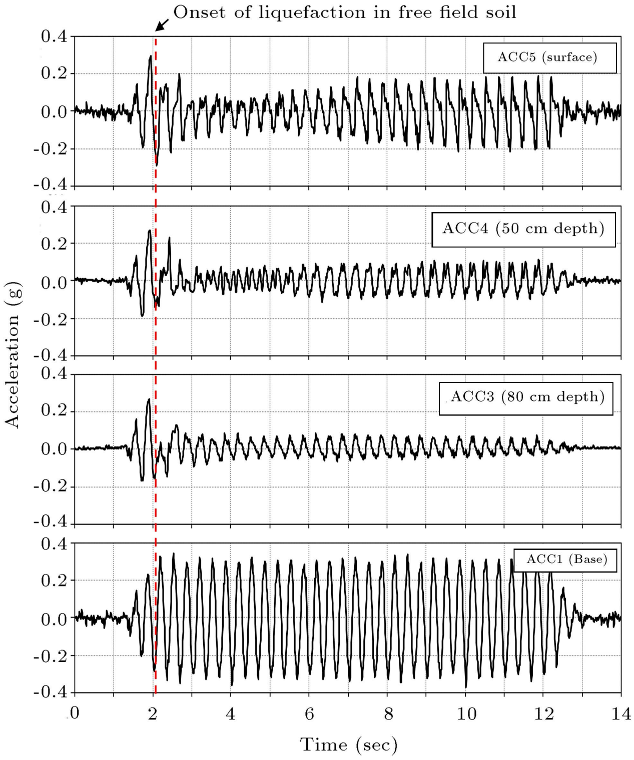

Figure 5. Time histories of acceleration in the free field soil (Model B).

Time histories of the acceleration of the piles as well as the cap in Models A and B along with their response spectra are outlined in Figure 6. As observed in this figure, inclusion of the micropiles in the physical model increases the maximum pile cap acceleration from about 0.25 g in Model A to about 0.38 g in Model B. Moreover, the pile cap motion in Model B, produced higher spectral accelerations in low time periods and lower spectral accelerations in higher periods than those in Model A. Figure 6 shows the variation in accelerations along the piles in Model B, as designated by ACC6 and ACC7. The amplitude of the pile acceleration is somewhat larger than that recorded in the free field particularly at deeper depths. In addition, the recorded accelerations adjacent to the piles appear to contain higher frequencies than those of the free field accelerations. This is mainly due to the inclusion of micropiles in Model B which alters the resonance frequency of the model ground close to the piles and transfers the base shaking to

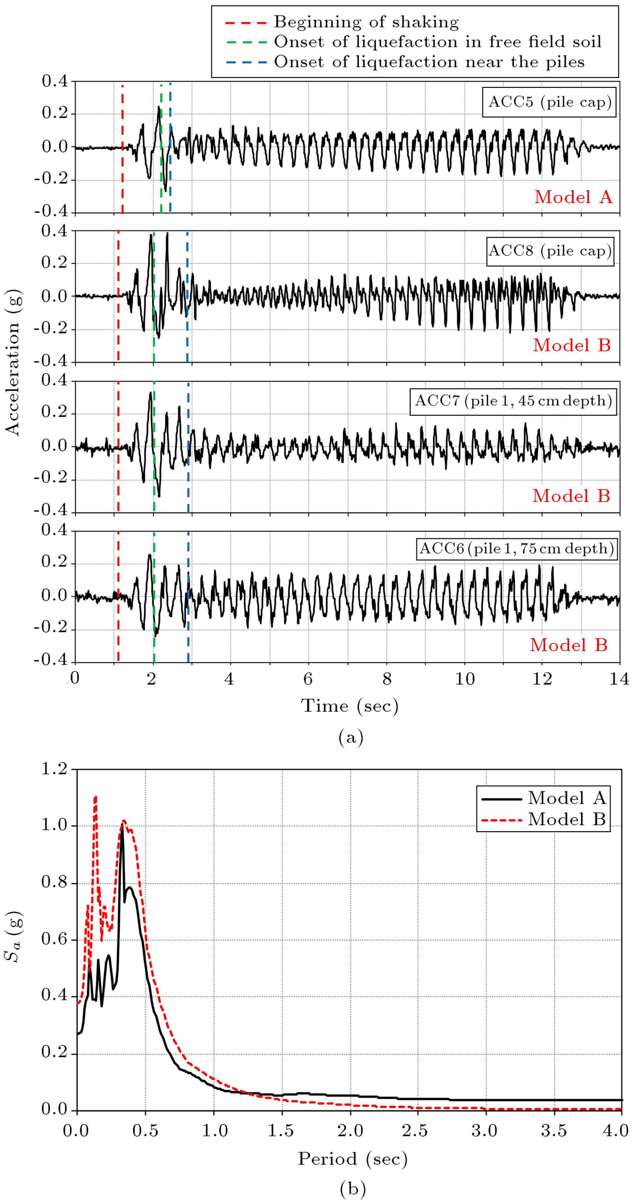

Figure 6. (a) Time histories of acceleration of the pile caps in Models A and B. (b) Response spectra of accelerations of the pile caps in Models A and B.

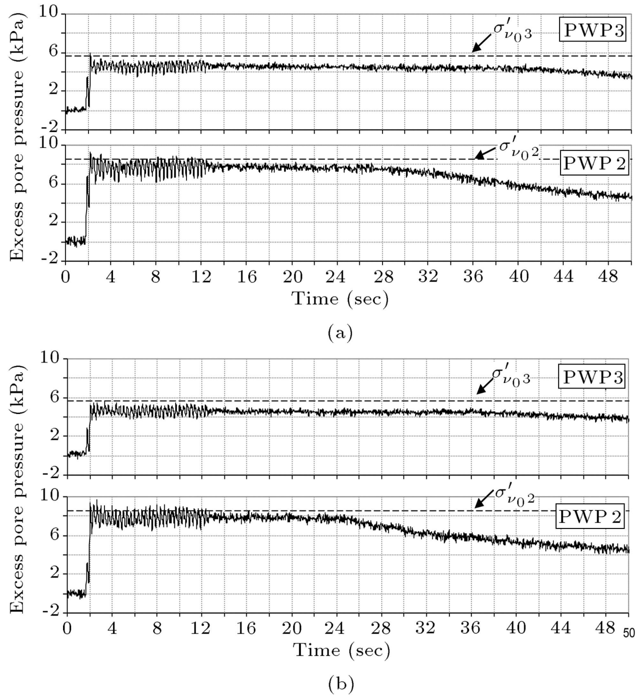

Figure 7. Excess pore pressure time histories in the free field soil: (a) Model A and (b) Model B.

the liquefiable layer and, then, up to the ground surface. The acceleration recorded at pile cap in both models reached its maximum value just before liquefaction initiation; however, after the liquefaction, the acceleration amplitude decreased since the liquefied soil considerably lost its shear strength, hence unable to transfer significant accelerations to the piles.

4. Excess pore water pressure records

The excess pore water pressures were monitored using miniature pore water pressure transducers located in the free field and near the pile group at different depths. Time histories of the recorded excess pore water pressures (in the free field) are listed in Figure 7. Due to the malfunctioning of PWP1 transducer during the experiment, it failed to record any PWP. According to Figure 7, the soil was liquefied after a few cycles of shaking in both models, indicating the low density (i.e., $D_r = 15\%$) of the middle liquefiable layer. In addition, liquefaction started sooner at shallower depths owing to the lower effective stress than that at the deeper soil. According to this figure, the dissipation of the excess pore water pressures initiated at deeper depths after the end of shaking. In other words, the consolidation of soil after liquefaction began at lower depths of the liquefiable layer.

Figure 8 presents the excess pore water pressures recorded in soil adjacent to the piles. According to this figure, the soil close to the upslope side of the piles was liquefied almost simultaneously with the free field soil while that located nearby the downslope side of the piles was liquefied with a small delay. Of note, such behavior was more clearly tracked during a similar shaking table test on stiff aluminum piles representing circular steel piles of 40 cm external diameter on the prototype scale, which was investigated by Haeri et al. [59]. Accordingly, it can be argued that the flexibility or rigidity of the piles affects the excess pore water pressure development in the vicinity of piles. In fact, the flexible piles of current experiments deflected together with the surrounding soil during the early stages of lateral spreading; therefore, the soil adjacent to the downslope side of the piles remained in contact with the piles, and it did not create a gap to act

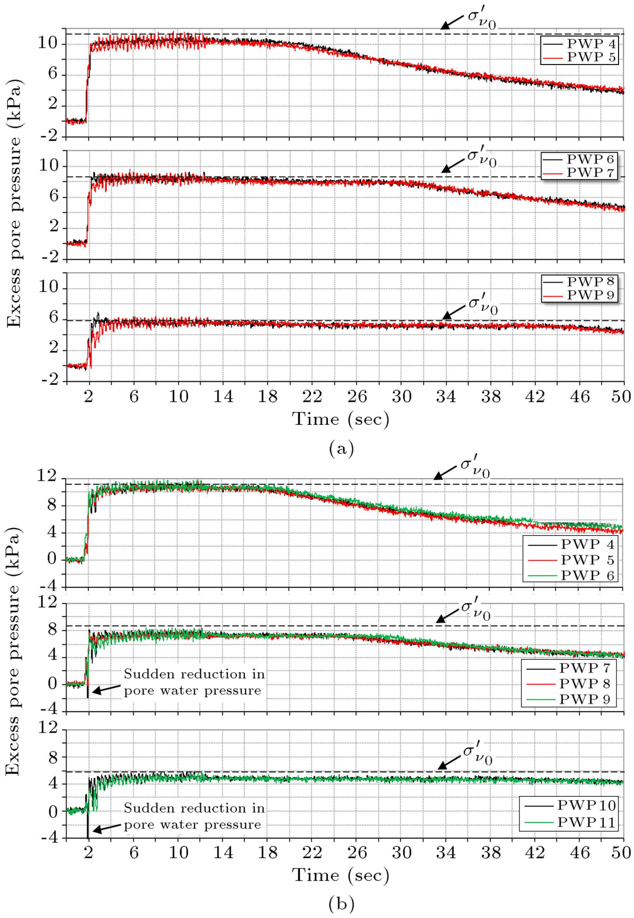

Figure 8. Excess pore pressure time histories close to the piles: (a) Model A and (b) Model B.

as a potential drainage path retarding generation of the excess pore water pressure. Evidence for such behavior is provided in Figure 9 where no obvious separation between the piles and soil adjacent to the downslope side of them is observed throughout the lateral movement of the liquefied soil. This issue is elaborated more in the next sections through sand boils occurring near a pile group consisting of stiff piles.

Dilation spikes observed in Figure 8(b) in the early stages of shaking can be attributed to the slight densification of the loose sand on the upslope side of pile group resulting from insertion of micropiles that consequently caused momentary minor dilative behavior of the soil during liquefaction. It should be noted that maximum pile accelerations occur almost simultaneously with the momentary suction in pore water pressures (Figure 10).

5. Bending moment records

As mentioned earlier, a number of strain gauges were attached to the model piles at different depths to record the bending moments in piles during lateral spreading. To eliminate the axial strains and maintain the bending strains, the strain gauges were configured in half Whetstone bridges.

The recorded bending moments in different piles in Models A and B are plotted in Figures 11 and 12, respectively. The sign convention of the bending moments can be followed in Figure 2. The bending moment data are presented on the model scale; however, they can be conveniently converted to the prototype scale using the scale similitude law, as given in Table 1. It should be noted that since the base shaking is applied parallel to the ground slope, the bending moment in piles contains a cyclic component due to the oscillating dynamic soil pressures on the piles as well as a monotonic component resulting from the permanent lateral deformation of the ground (i.e., lateral spreading) and its associated kinematic lateral pressures. Since this study puts its main focus on the kinematic soil pressures induced by lateral spreading, the bending moment data was separated into cyclic and monotonic components. For this purpose, monotonic components of the bending moments were extracted by filtering out their cyclic components using a low-pass filter.

The monotonic components of the bending moment data are shown in Figures 11 and 12 in thick lines. Based on these figures, one can notice that in both models, the bending moments in piles increase to their maximum values and, then, decrease as the liquefied soil loses its shear strength, thus allowing the piles to rebound due to their elastic stiffness.

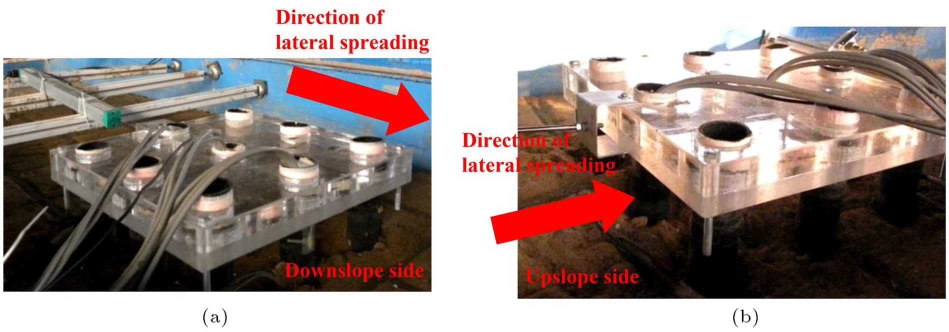

Figure 9. Photos of the soil adjacent to the piles in Model A: (a) Downslope side of the pile group and (b) upslope side of the pile group.

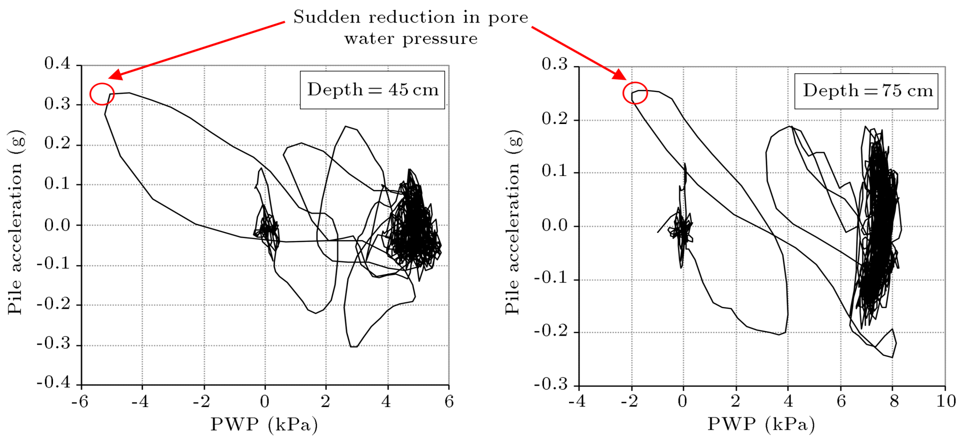

Figure 10. Variations in pile acceleration with pore water pressure at two different depths along the pile (P1) in Model B.

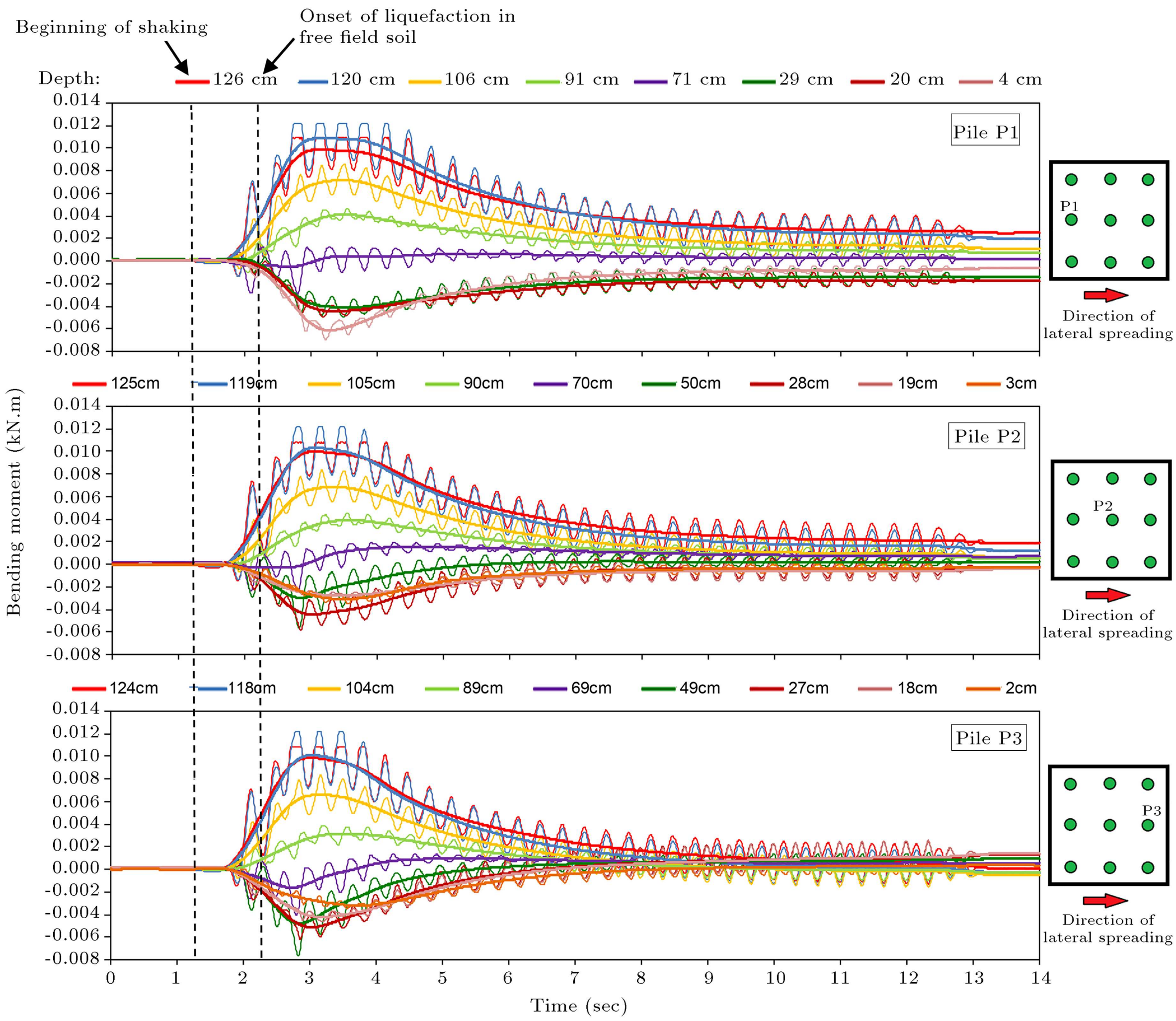

Figure 11. Time histories of the bending moments at different depths of piles in Model A (thick smooth lines show the monotonic components of bending moments).

Variations of the monotonic component of the recorded bending moments with depth for different piles in both Models A and B are presented in Figures 13 and 14, respectively. The variations indicate that while the bending moments at shallower depths are negative, those at deeper depths are positive. While comparing the bending moment profiles in piles located at the same locations in Models A and B, no significant difference was observed, indicating that the adopted micropile system was not that much effective

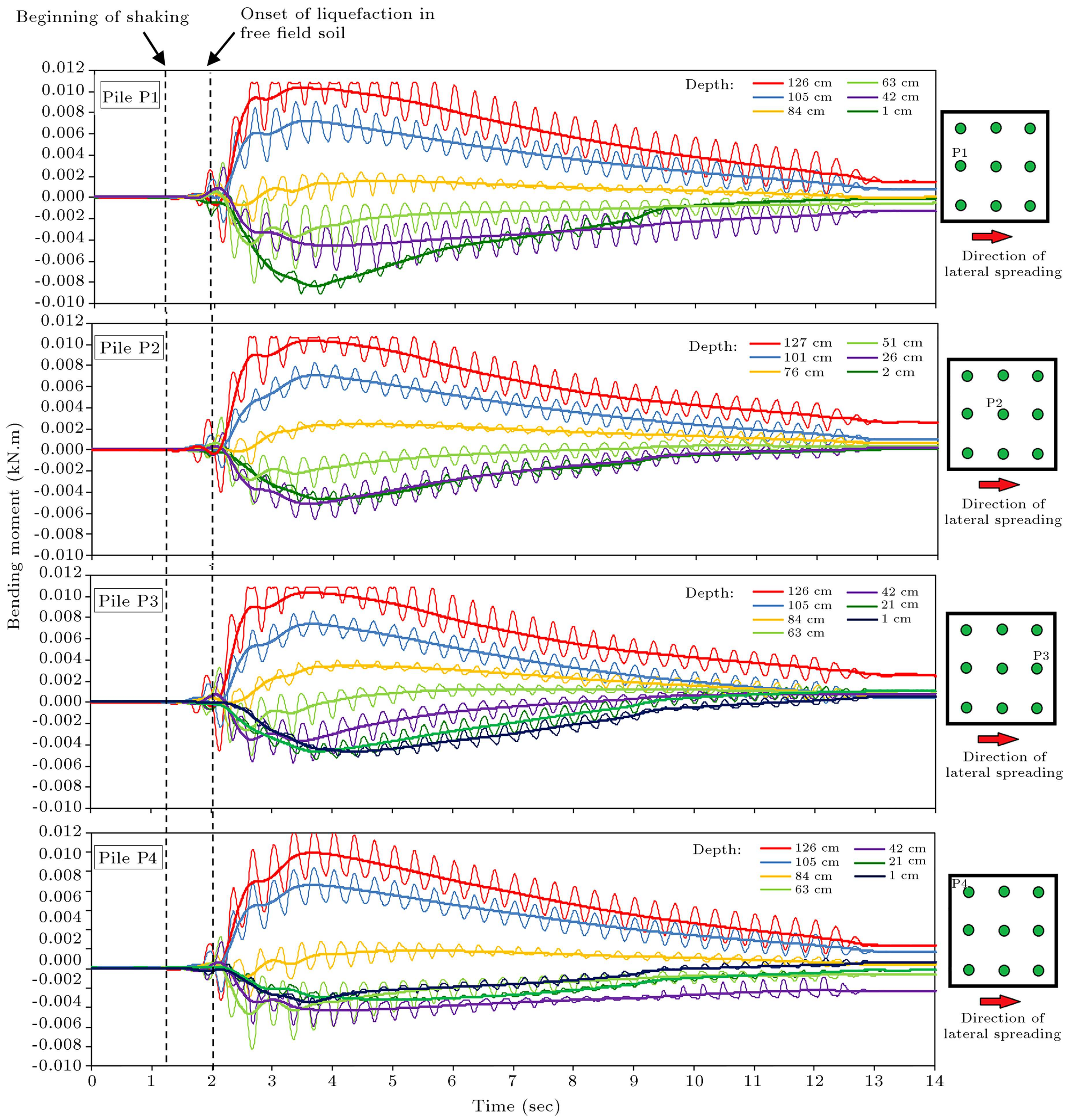

Figure 12. Time histories of the bending moments at different depths of piles in Model B (thick smooth lines show the monotonic components of bending moments).

in reducing the induced bending moments in piles. The residual bending moments observed in Model A after the peak point (i.e., at $t = 8.0$ sec and $t = 12.0$ sec) resulted from the effects of micropiles near the upslope side of the pile group, which prevented complete return of the pile group towards the upslope.

6. Relative displacements of the soil and the pile caps

Time histories of the lateral displacement of ground surface in free field areas of Models A and B are shown in Figure 15. As observed, the soil in both models started to move downslope upon liquefaction initiation. The maximum value of the ground surface displacements is about 10 cm in both physical models.

During the experiments, a series of successive photographs were taken from the side of the physical models during shaking. The profiles of the lateral displacements of soil were then obtained by analyzing these images and tracking the lateral displacement of the columns of colored sand created behind the transparent Plexiglas windows on the side of the model container (Figure 3). These displacement profiles are depicted in Figure 16. The maximum lateral displacements of the ground, observed at the middle depths of the liquefied layer, are about 14 cm and 15 cm for Models A and B, respectively. Moreover, the lateral

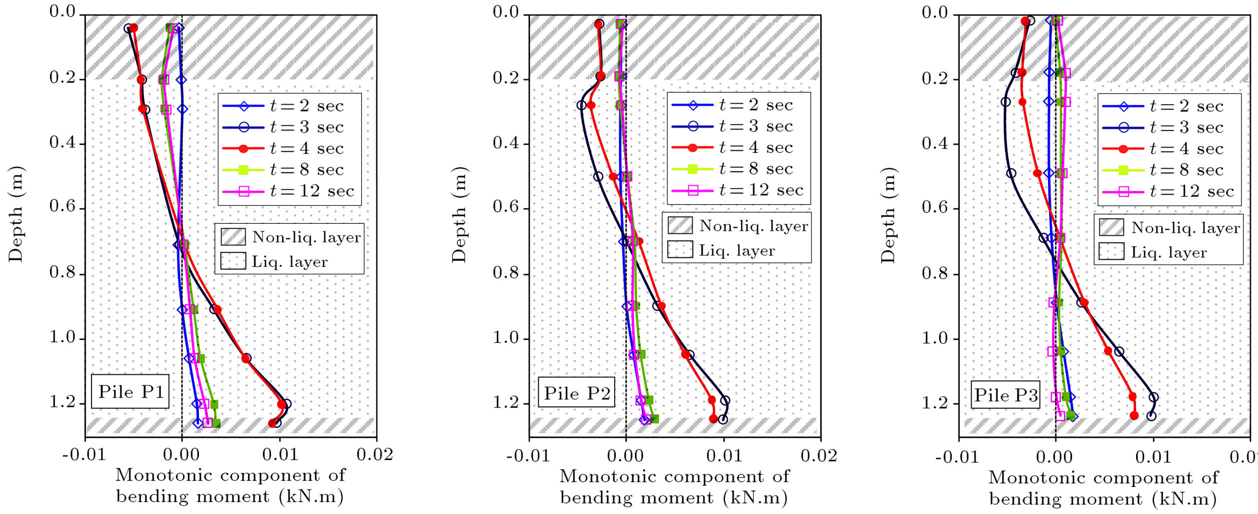

Figure 13. Profiles of the monotonic component of the bending moments along the piles in Model A.

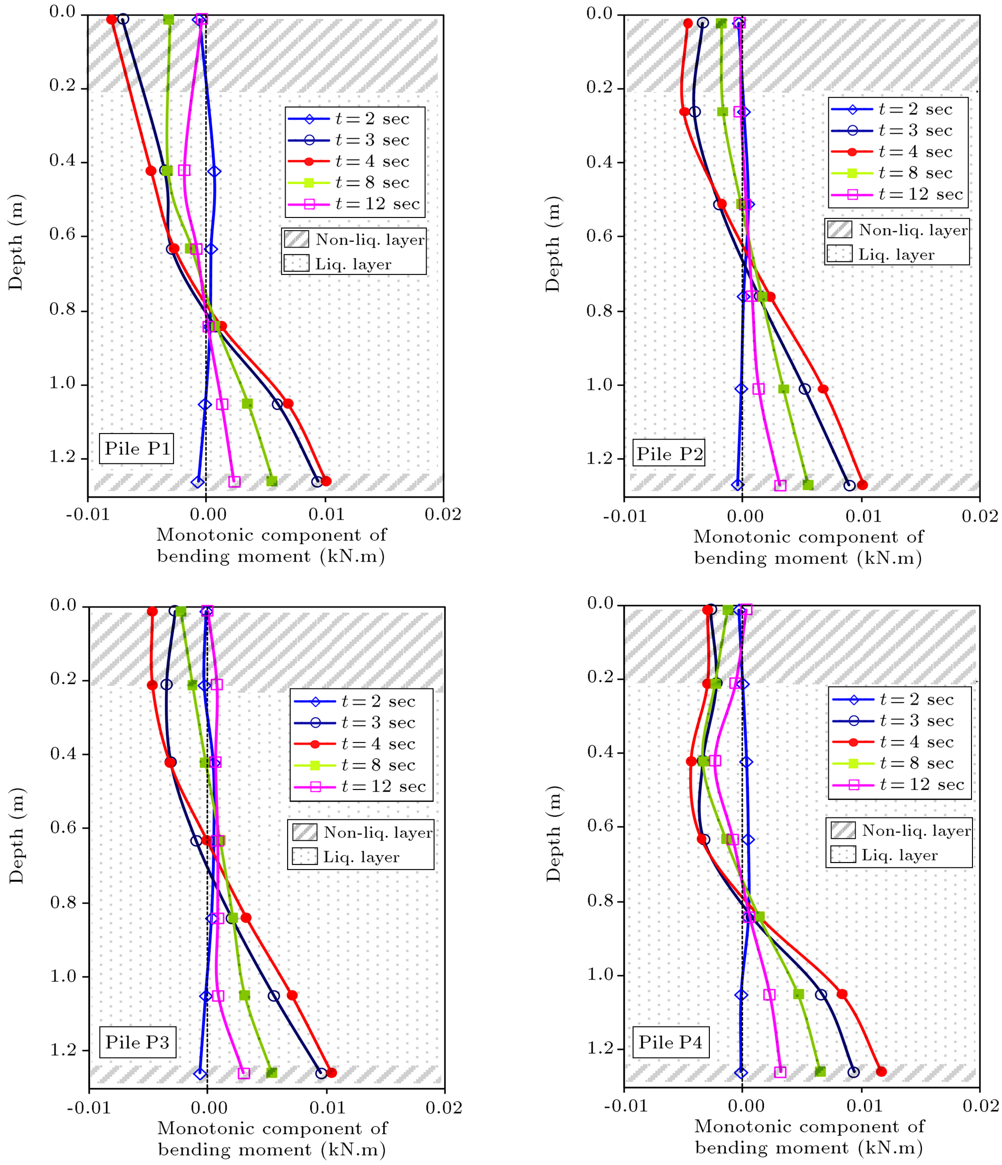

Figure 14. Profiles of the monotonic component of the bending moments along the piles in Model B.

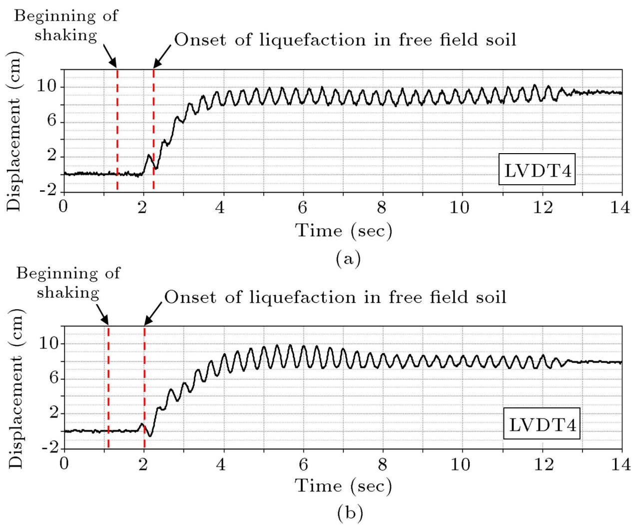

Figure 15. Time history of the lateral displacement of ground surface in the free field area: (a) Model A and (b) Model B.

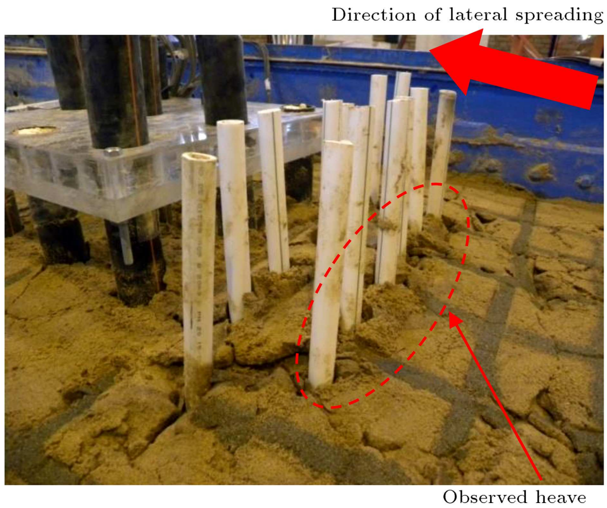

Figure 17. Photo of the upslope side of the micropiles in Model B.

displacements within the middle depths of the liquefied layer are rather uniform while they are reduced near the boundaries of the upper and lower non-liquefiable layers. A comparison between the results in Figure 16 shows that the value of soil displacement at the upper depths of Model B is generally lower than that in Model A. This is the reason why the employed micropiles restricted the lateral movement of the upper non-liquefiable layer and, to some extent, that of the upper depths of the liquefiable layer. However, at deeper depths of the liquefiable layer, the micropiles did not restrict the lateral movement of the liquefied soil. This behavior appears to be a typical behavior of piles under lateral loading known as wedge-type failure versus flow-type failure. In the upper non-liquefiable layer, the lateral resistance mechanism is three-dimensional, producing a wedge-shaped passive failure mechanism. With depth, as the liquefiable soil loses most of its shear strength, the failure mechanisms resolve into the flow-type failure mechanism, which is indicative of a two-dimensional phenomenon. As a result, one possible solution to enhance the efficiency of the micropile system in mitigating the effect of lateral spreading is to include more micropiles with smaller center-to-center spacing or insert additional rows of micropiles to restrict the lateral flow of liquefiable soil more effectively. Other mitigation enhancements are out of the scope of this study, hence neglected. Figure 17 indicates the slight heave on the ground surface on the upslope side of the micropiles that refers to the evidence for the relative resistance of micropiles

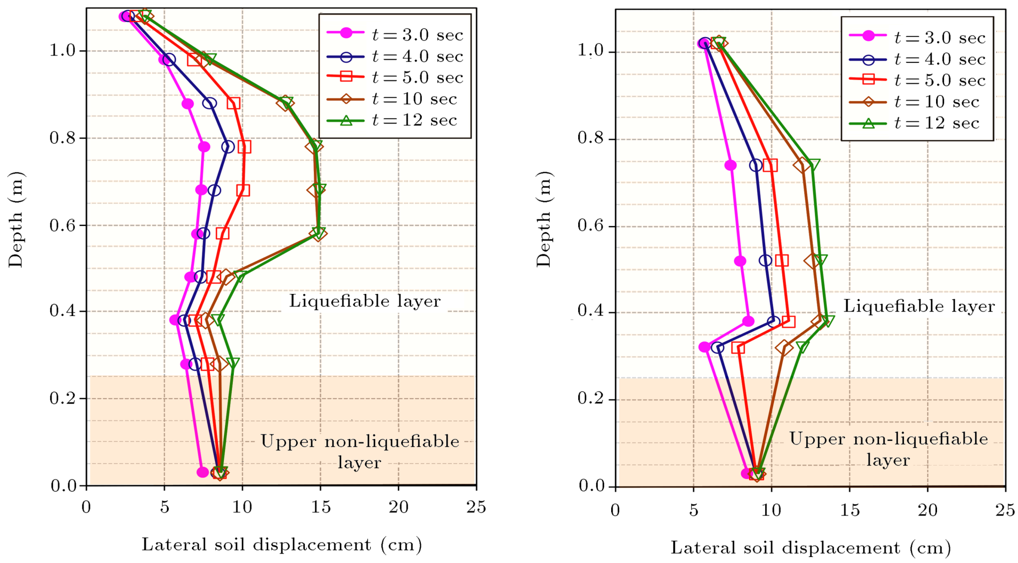

Figure 16. Profiles of the lateral displacement of soil at representative snapshots during shaking for (a) Model A and (b) Model B.

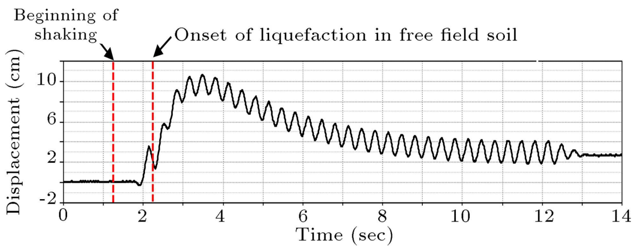

Figure 18. Time history of the pile cap displacement in Model A.

against the downslope movement of the upper non-liquefiable layer.

Figure 18 displays the time history of the pile cap displacement in Model A. According to this figure, the pile cap started moving downslope along with the soil until reaching the maximum amount of displacement (about 10.4 cm). Then, at the peak displacement point, elastic forces of the piles overcame the shear strength of the liquefied soil. As a result, the pile cap started returning to its initial position while the soil was still moving downslope in the free field (comparing Figures 18 and 15(a). Since displacement transducer in Model B malfunctioned, no useful data was recorded for that Model in this respect. However, photographs taken from the top of Model B were analyzed to measure the maximum displacement of the pile cap by tracking its lateral movement. The results revealed that the pile cap displacement in Model B was about 10 cm, which was about 0.4 cm smaller than the corresponding value in Model A. This small reduction of pile cap displacement in Model B resulted from the restriction imposed by the micropiles on the lateral displacement of the upper non-liquefiable layer and consequently its lateral pressure on the model piles.

7. Lateral pressure of liquefied soil

The lateral pressures of the liquefied soil exerted on the piles during lateral spreading can be obtained by double differentiation of the recorded bending moments in piles, as illustrated in Eq. (3):

$$P[z,t] = \frac{\partial^2 M[z,t]}{\partial z^2}, \tag{3}$$

where $M[z,t]$ and $P[z,t]$ are the time histories of bending moment and lateral pressure in pile, respectively, at depth z. Given that possibility of any error in the bending moment data would increase during the differentiation procedure, different numerical methods such as weighted residual or curve fitting techniques were suggested to reduce these errors in differentiation of bending moment data. Here, the weighted residual method proposed by Brandenberg et al. [60] was employed to calculate the soil pressures from the recorded bending moments. This method functions based on minimization of the weighted residuals similar to that usually performed in the finite element method. Brandenberg et al. [60] concluded that their proposed procedure could yield more accurate results than those using common curve fitting techniques. Further details of this method are provided in [60].

Figures 19 and 20 show the profiles of the lateral soil pressure exerted on different piles in Models A and B, respectively. In order to calculate the kinematic pressures caused by lateral spreading, monotonic components of the bending moments were employed. Figures 19 and 20 list the soil pressures suggested by JRA [58].

JRA [58] stipulates the application of 30% of the total overburden pressure to the outmost width of pile group as the exerted lateral pressures on piles in any desired depth within the liquefiable layer. According to this code, in the case of the existence of an upper non-liquefiable layer, the associated passive lateral pressure of this layer should also be imposed on the piles. In addition, it is a common practice to assume that the

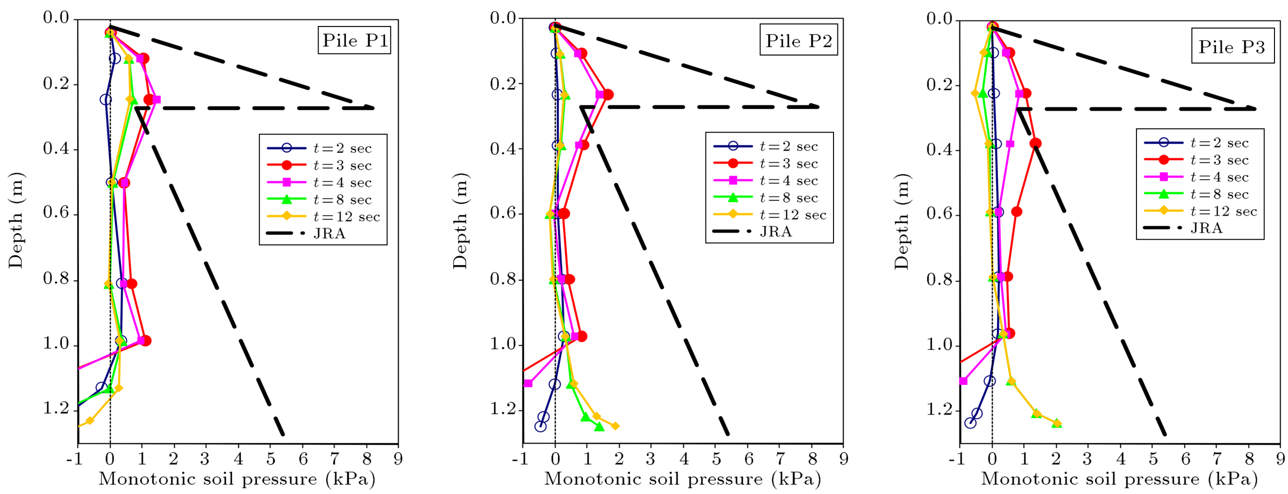

Figure 19. Profiles of soil pressure exerted on the piles due to lateral spreading in Model A.

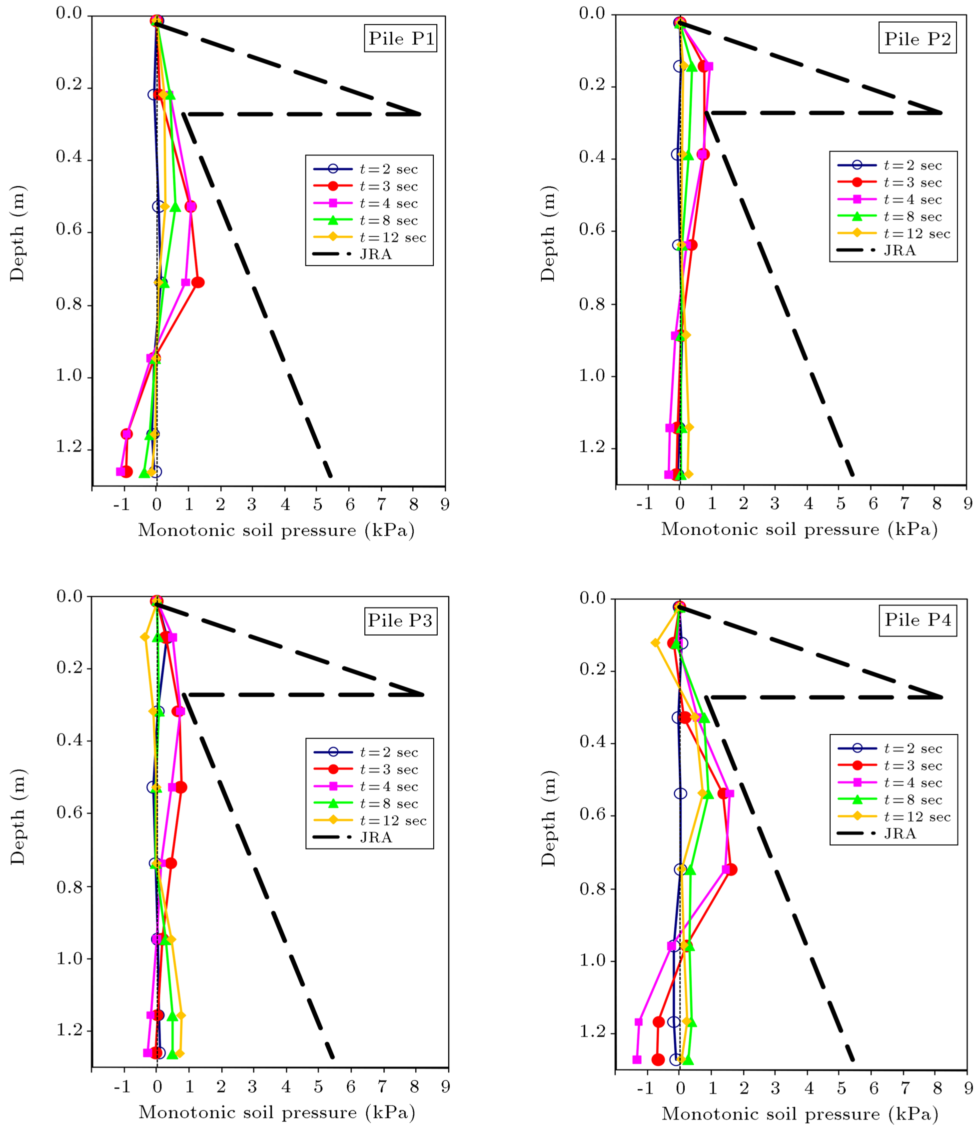

Figure 20. Profiles of soil pressure exerted on the piles due to lateral spreading in Model B.

total lateral force applied to the pile group is equally shared among individual piles in the group. Herein, the lateral pressure recommended by JRA [58] is exerted on the whole width of the pile group (i.e., 35 cm) to calculate the total lateral force at any desired depth; then, this lateral force is equally shared among nine individual piles of the group. Moreover, in the case of an upper non-liquefiable layer, a passive soil pressure was exerted on the pile group as per JRA [58].

According to Figures 19 and 20, the exerted lateral pressures in both models were considerably lower than those suggested by JRA [58], mainly because the piles used in this study were flexible representing RC piles in prototype (compared to the prototype stiff steel piles as previously tested by Haeri et al. [59]); however, JRA [58] did not consider the flexural stiffness (EI) of the piles in its formulations. According to Figure 20, the lateral pressure exerted on the upslope piles (P1 and P4) caused by the upper non-liquefiable layer in Model B is lower than that in Model A. However, this is not the case for both middle and downslope piles. These observations showed that the micropiles restricted the movement of upper non-liquefiable layer; yet, they did not effectively reduce the movement of the liquefiable layer and associated lateral pressures on the piles.

Time histories of the total forces exerted on the piles can be obtained through integration of the lateral pressures on the piles:

$$F_{L.L_i}[t] = \int_{z=0}^{z=H_1} P_i[z,t]dz,$$

$$F_{N.L_i}[t] = \int_{z=H_1}^{z=H_1+H_2} P_i[z,t]dz. \qquad (4)$$

In Eq. (4), $F_{L.L_i}[t]$ and $F_{N.L_i}[t]$ are the time histories

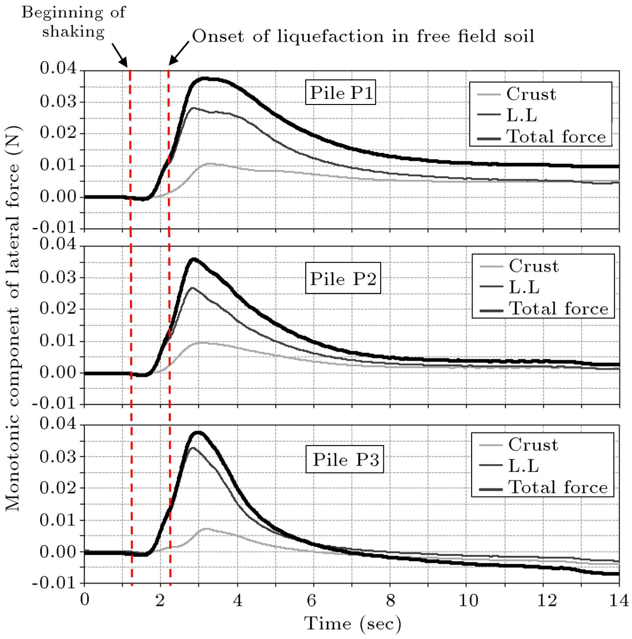

Figure 21. Time histories of the monotonic component of the exerted lateral forces on piles in Model A.

of the lateral forces exerted on pile i due to liquefiable and upper non-liquefiable layers, respectively. H_1 is the thickness of liquefiable layer and H_2 the thickness of the upper non-liquefiable layer. The time histories of monotonic component of the exerted lateral forces on the piles are plotted in Figures 21 and 22. In these figures, the lateral forces in both models increase within the first few cycles of excitation, thus reaching the peak value. Then, they decrease as the piles return to their initial position. This reduction occurs faster on the downslope pile (P3) than that on the upslope pile (P1). In addition, in both figures, the peak value of the exerted lateral force on the middle pile (P2) is lower than those on the upslope and downslope piles (P1 and P3).

Figure 23 makes a comparison between the maximum values of the total lateral forces on different model piles and those separately exerted by the upper non-liquefiable as well as the liquefiable layers. The difference between the maximum values of the total lateral forces on both upslope (P1) and downslope (P3) piles in Model A is negligible; however, the maximum lateral force on upslope pile (P1) in Model B is slightly larger than that exerted on downslope pile (P3). This possibly results from the slight densification of the upslope soil adjacent to pile P1 in Model B while inserting the micropiles.

The effectiveness of the micropiles can be assessed by comparing the lateral forces exerted on individual piles in Models A and B with identical locations in the group. The comparison results revealed that the micropiles could reduce the lateral force due to upper non-liquefiable layer on piles of Model B. This reduc-

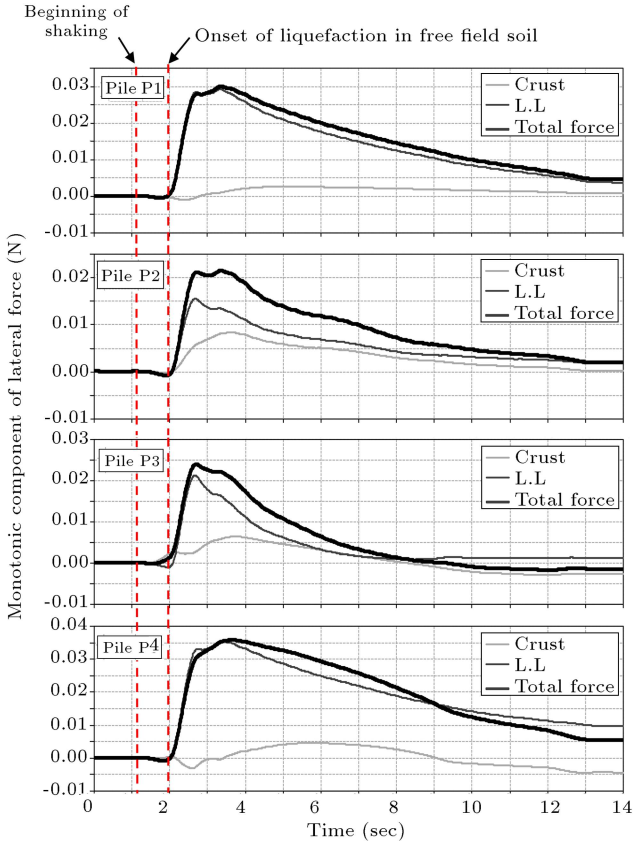

Figure 22. Time histories of the monotonic component of the exerted lateral forces on piles in Model B.

tion was more significant in the upslope pile (P1) of the group. The lateral forces caused by the liquefiable layer were also smaller in Model B than those in Model A. Such a reduction was observed mainly because the lateral forces in Model B within the lower half of the liquefiable layer were negative (i.e., passive).

The total lateral forces on the pile groups can be calculated based on Eqs. (5) and (6):

$$F_{row_j}[t] = \sum_{i=1}^{3} F_{ij}[t], \tag{5}$$

$$F_{total}[t] = \sum_{j=1}^{3} F_{row_j}[t], \tag{6}$$

where $F_{ij}[t]$, $F_{row_j}[t]$, and $F_{total}[t]$ are the time histories of the total lateral forces on each individual pile in the group located at the jth row, each row of the piles, and the whole group, respectively. Of note, only three piles in Model A were instrumented (P1, P2, and P3). In this regard, to calculate the total force exerted on the pile group, it was assumed that the side piles of each row received 1.26 times the lateral forces exerted on the middle pile of the row due to the neighboring effect, as observed in the previous experiment on 3×3 pile group performed by Haeri et al. [59]. Only four

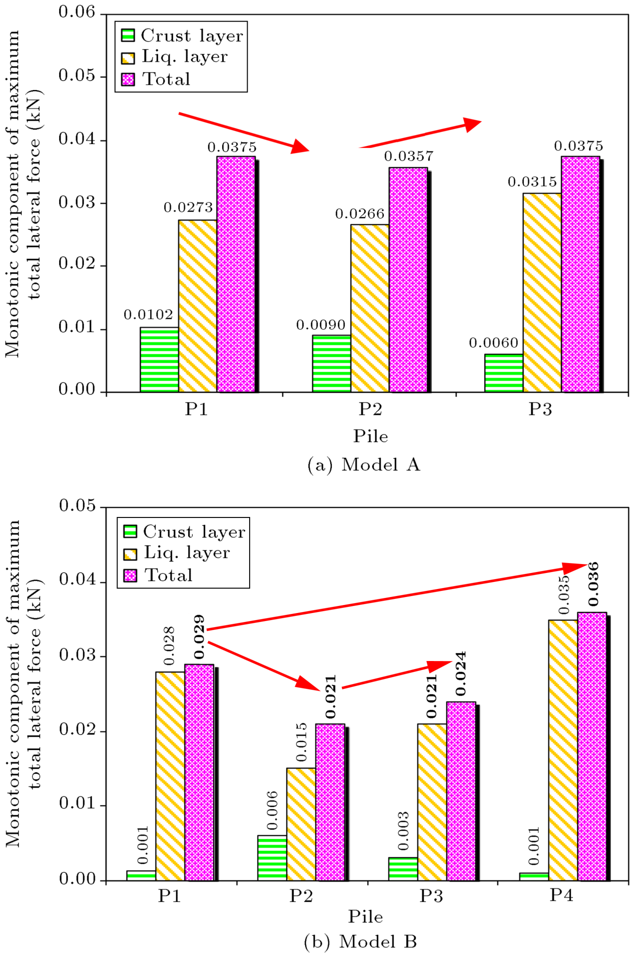

(a) Model A

(b) Model B

Figure 23. Maximum lateral forces exerted on the model piles.

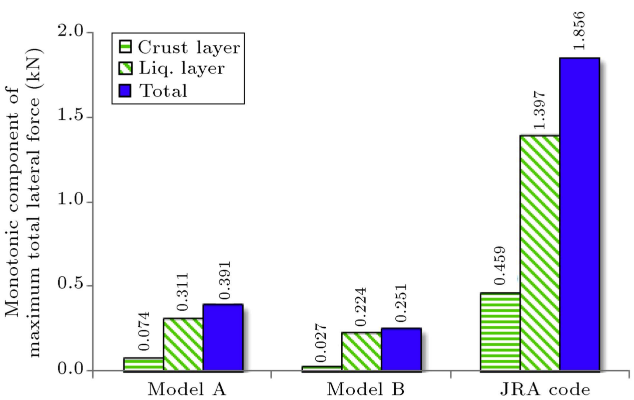

Figure 24. Maximum total lateral forces exerted on the pile groups along with the values suggested by JRA [58] code.

piles were instrumented (P1, P2, P3, and P4) in Model B. However, due to the axial symmetry of this model in plan, it is expected that the ratio of exerted force on piles P1 to P4 be used to calculate the forces exerted on other side piles of the pile group, which are not already instrumented. Figure 24 compares the maximum total lateral forces exerted on the pile group in each model with the values calculated based on JRA [58]. As observed, the values predicted by the JRA [58] were significantly higher than those obtained in current experiments, mainly due to the flexibility of the model piles.

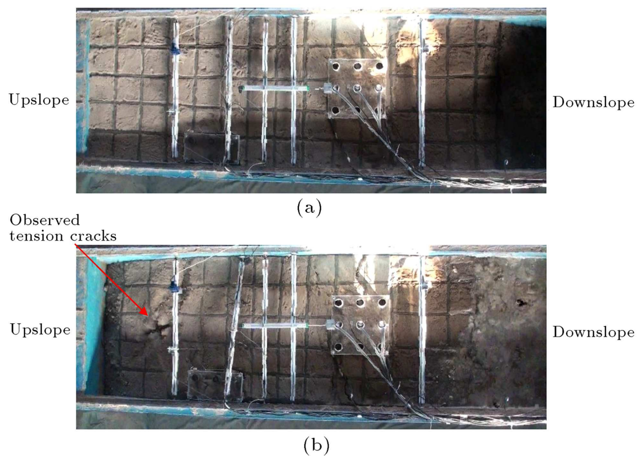

Figure 25. Photos of the surface of Model A: (a) Before shaking and (b) just after the end of shaking.

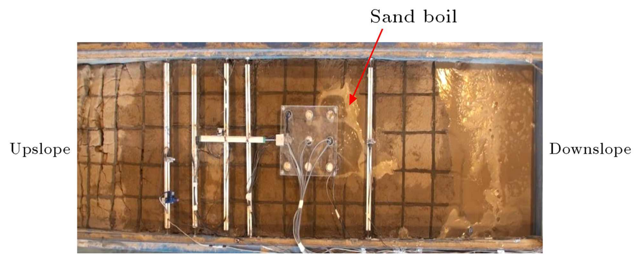

Figure 26. Ground surface in a physical model test on a stiff pile group only after the end of shaking [59].

8. Further observations

During the experiments, a high-resolution camcorder was mounted on the top of the physical models. The movies recorded by this camcorder were extracted into a series of sequential photographs, thus providing very useful information on the deformations of the ground surface and piles during lateral spreading. Figure 25 depicts two photos of the ground surface in Model A before excitation and just after the end of the excitation. Deep tension cracks observed in the free field ground on the upslope side were indicative of the substantial lateral ground movement and settlement. Figure 26 depicts a photo of a physical model test performed on a pile group configured similar to the pile group in the current study but with stiffer aluminum piles [59]. As observed in that test, considerable sand boil occurred in the vicinity of the downslope side of the pile group, yet no sand boil was detected at the same location in Figure 25, confirming that no separation occurred between the liquefied soil and the flexible piles in Model A situated on the downslope side of the pile group.

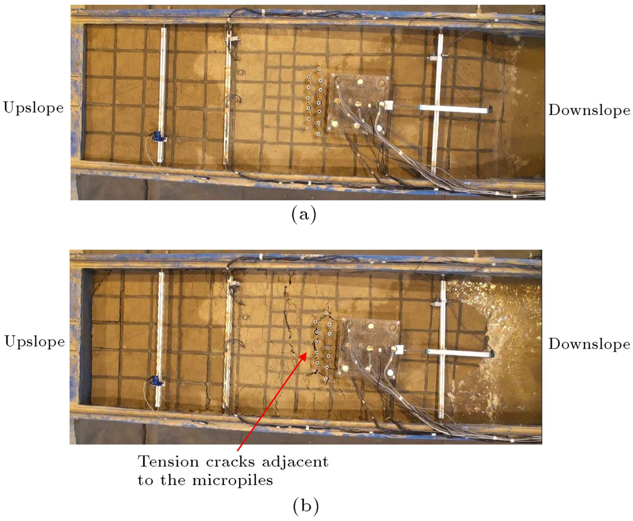

Figure 27. Photos of the ground surface in Model B: (a) Before the shaking and (b) just after the end of shaking.

Figure 27 illustrates two photographs of the plan view of the ground surface in Model B. As observed, the micropiles and soil adjacent to them were separated from the rest of the ground by tension cracks. This is possibly because of the slight densification of the soil adjacent to the micropiles, relative to the soil in the rest of the model that created two different zones with different behavior.

9. Conclusions

In this study, two large-scale shake table tests on 3×3 flexible pile groups were performed to evaluate the effectiveness of the vertical micropiles inserted in a liquefiable sandy layer as a countermeasure to reduce the lateral force resulting from lateral spreading. To this end, a model without any mitigation strategy and a model remediated with micropiles were tested and compared with each other. The main findings of the current research are highlighted in the following:

- The employed micropile system was not effective enough to reduce the induced lateral pressures and bending moments in the piles. On the other hand, it could increase the accelerations transferred to the pile cap (or the superstructure) and alter the resonance frequency of the model ground close to the piles;
- The employed micropiles could also decrease the soil pressure exerted by the upper non-liquefiable layer on the upslope piles of the group. However, they did not effectively decrease the lateral pressures exerted by the liquefiable layer on the piles;
- The exerted lateral pressures on the piles in both models were considerably lower than those suggested by Japan Road Association (JRA) [58] owing to the flexibility of the model piles;
- Soil displacement at the upper depths of the model remediated with micropiles is generally lower than that in model with no mitigation measure, indicating that the employed micropiles restricts the lateral displacement of upper non-liquefiable layer and partially that of the upper depths of the liquefiable layer. However, this restriction remains not noticeable at deeper depths of the liquefiable layer. Several solutions can be considered to more effectively restrict the movement of liquefied soil and decrease the lateral soil pressure on piles under strong ground motions such as using the micropiles in a tighter pattern, adopting stiffer ones and fixing them in the underlying non-liquefiable layer. Of note, a detailed effectiveness of the mentioned solutions needs further investigations in the future;
- The excitation applied to the model in this study was equivalent to a relatively strong ground shaking. As a result, more possible effectiveness of the micropiles for lateral spreading remediation under weaker ground motions needs to be investigated in future studies. Numerical simulations can also be undertaken in this respect.

References

1. Hamada, M., Yasuda, S., Isoyama, R., et al. "Study on liquefaction induced permanent ground displacements", Report for the Association for the development of Earthquake Prediction (1986).
2. Bardet, J.P. and Kapuskar, M. "Liquefaction sand boils in San Francisco during 1989 Loma Prieta earthquake", *J. Geotech. Eng.*, **119**(3), pp. 543–562 (1993).
3. Hamada, M., Isoyama, R., and Wakamatsu, K. "Liquefaction-induced ground displacement and its related damage to lifeline facilities", *Soils & Found.*, **36** (special issue), pp. 81–97 (1996).
4. Tokimatsu, K., Mizuno, H., and Kakurai, M. "Building damage associated with geotechnical problems", *Soils & Found.*, **36** (special issue), pp. 219–234 (1996).
5. Tokimatsu, K. and Asaka, Y. "Effects of liquefaction-induced ground displacements on pile performance in the 1995 Hyogoken-Nambu earthquake", *Soils & Found.*, **38** (special issue), pp. 163–177 (1998).
6. Tokimatsu, K., Tamura, S., Suzuki, H., et al. "Building damage associated with geotechnical problems in the 2011 Tohoku Pacific Earthquake", *Soils & Found.*, **52**(5), pp. 956–974 (2012).
7. Eberhard, M.O., Baldridge, S., Marshall, J., et al. "Mw 7.0 Haiti earthquake of January 12, 2010", USGS/EERI Advance Reconnaissance Team Report (2013).
8. Kramer, S. and Elgamal, A. "Modeling soil liquefaction hazards for performance based earthquake engineering", Report 2001/13, Pacific Earthquake Engineering Research Center, University of California, Berkeley (2001).

9. Hamada, M. "Performances of foundations against liquefaction-induced permanent ground displacements", *12th World Conference on Earthquake Engineering*, Tokyo, Japan, pp. 1754–1761 (2000).

10. Cubrinovski, M., Kokusho, T., and Ishihara, K. "Interpretation from large-scale shake table tests on piles undergoing lateral spreading in liquefied soils", *Soil Dyn. Earthq. Eng.*, **26**(2–4), pp. 275–286 (2006).

11. Dungca, J.R., Kuwano, J.I., Takahashi, A., et al. "Shaking table tests on the lateral response of a pile buried in liquefied sand", *Soil Dyn. Earthq. Eng.*, **26**(2–4), pp. 287–295 (2006).

12. He, L., Elgamal, A., Abdoun, T., et al. "Liquefaction-induced lateral load on pile in a medium D_r sand layer", *J. Earthq. Eng.*, **13**(7), pp. 916–938 (2009).

13. Motamed, R., Sesov, V., Towhata, I., et al. "Experimental modeling of large pile groups in sloping ground subjected to liquefaction-induced lateral flow: 1-G shaking table tests", *Soils & Found.*, **50**(2), pp. 261–279 (2010).

14. Haeri, S.M., Kavand, A., Rahmani, I., et al. "Response of a group of piles to liquefaction-induced lateral spreading by large scale shake table testing", *Soil Dyn. Earthq. Eng.*, **38**, pp. 25–45 (2012).

15. Motamed, R., Towhata, I., Honda, T., et al. "Pile group response to liquefaction-induced lateral spreading: E-Defense large shake table test", *Soil Dyn. Earthq. Eng.*, **51**, pp. 35–46 (2013).

16. Kavand, A., Haeri, S.M., Asefzadeh, A., et al. "Study of the behavior of pile groups during lateral spreading in medium dense sands by large scale shake table test", *Int. J. Civ. Eng.*, **12**(3–B), pp. 186–203 (2014).

17. Abdoun, T. and Dobry, R. "Evaluation of pile foundation response to lateral spreading", *Soil Dyn. Earthq. Eng.*, **22**(9–12), pp. 1051–1058 (2002).

18. Haigh, S.K. and Madabhushi, S.P. "Centrifuge modelling of lateral spreading past pile foundations", *International Conference on Physical Modelling in Geotechnics*, St. John's, Newfoundland, Canada (2002).

19. Abdoun, T., Dobry, R., O'Rourke, T.D., et al. "Pile response to lateral spreads: centrifuge modeling", *J. Geotech. Geoenviron.*, **129**(10), pp. 869–878 (2003).

20. Imamura, S., Hagiwara, T., Tsukamoto, Y., et al. "Response of pile groups against seismically induced lateral flow in centrifuge model tests", *Soils & Found.*, **44**(3), pp. 39–55 (2004).

21. Brandenberg, S.J., Boulanger, R.W., Kutter, B.L., et al. "Behavior of pile foundations in laterally spreading ground during centrifuge tests", *J. Geotech. Geoenviron.*, **131**(11), pp. 1378–1391 (2005).

22. Gonzalez, L., Abdoun, T., and Dobry, R. "Effect of soil permeability on centrifuge modeling of pile response to lateral spreading", *J. Geotech. Geoenviron.*, **135**(1), pp. 62–73 (2009).

23. Ashford, S.A., Juirnarongrit, T., Sugano, T., et al. "Soil-pile response to blast-induced lateral spreading. I: field test", *J. Geotech. Geoenviron.*, **132**(2), pp. 152–162 (2006).

24. Balakrishnan, A. and Kutter, B.L. "Settlement, sliding, and liquefaction remediation of layered soil", *J. Geotech. Geoenviron.*, **125**(11), pp. 968–978 (1999).

25. Abdoun, T., Dobry, R., Zimmie, T.F., et al. "Centrifuge research of countermeasures to protect pile foundations against liquefaction-induced lateral spreading", *J. Earthq. Eng.*, **9**, pp. 105–125 (2005).

26. Pamuk, A., Gallagher, P.M., and Zimmie, T.F. "Remediation of piled foundations against lateral spreading by passive site stabilization technique", *Soil Dyn. Earthq. Eng.*, **27**(9), pp. 864–874 (2007).

27. O'Donnell, S.T., Rittmann, B.E., and Kavazanjian Jr, E. "MIDP: Liquefaction mitigation via microbial denitrification as a two-stage process. I: Desaturation", *J. Geotech. Geoenviron.*, **143**(12), p. 04017094 (2017).

28. O'Donnell, S.T., Kavazanjian Jr, E., and Rittmann, B.E. "MIDP: Liquefaction mitigation via microbial denitrification as a two-stage process. II: MICP", *J. Geotech. Geoenviron.*, **143**(12), p. 04017095 (2017).

29. Olarte, J.C., Dashti, S., Liel, A.B., et al. "Effects of drainage control on densification as a liquefaction mitigation technique", *Soil Dyn. Earthq. Eng.*, **110**, pp. 212–231 (2018).

30. Huang, Y., Wen, Z., Wang, L., et al. "Centrifuge testing of liquefaction mitigation effectiveness on sand foundations treated with nanoparticles", *Eng. Geol.*, **249**, pp. 249–256 (2019).

31. Shen, M., Juang, C.H., and Chen, Q. "Mitigation of liquefaction hazard by dynamic compaction – A random field perspective", *Can. Geotech. J.*, **56**(12), pp. 1803–1815 (2019).

32. Salvatore, E., Modoni, G., Mascolo, M.C., et al. "Experimental evidence of the effectiveness and applicability of colloidal nanosilica grouting for liquefaction mitigation", *J. Geotech. Geoenviron.*, **146**(10), p. 04020108 (2020).

33. Mousavi, S. and Ghayoomi, M. "Liquefaction mitigation of sands with nonplastic fines via microbial-induced partial saturation", *J. Geotech. Geoenviron.*, **147**(2), p. 04020156 (2021).

34. Arango, I. "Mitigation of lateral ground displacements of liquefied soils with underground barriers", *Soil Dyn. Earthq. Eng.*, **22**(9–12), pp. 1067–1073 (2002).

35. Yasuda, S. and Ogasawara, M. "Studies on several countermeasures against liquefaction-induced flow and an application of a measure to existing bridges in Tokyo", *J. Jpn. Association. Earthq. Eng.*, **4**(3), pp. 370–376 (2004).

36. Motamed, R. and Towhata, I. "Mitigation measures for pile groups behind quay walls subjected to lateral flow of liquefied soil: Shake table model tests", *Soil Dyn. Earthq. Eng.*, **30**(10), pp. 1043–1060 (2010).

37. Kavand, A., Haeri, S.M., Raisianzadeh, J., et al. "Performance evaluation of stone columns as mitigation measure against lateral spreading in pile groups using shake table tests", *International Conference on Ground Improvement and Ground Control*, Wollongong, Australia (2012).

38. Salem, Z.B., Frikha, W., and Bouassida, M. "Effects of densification and stiffening on liquefaction risk of reinforced soil by stone column", *J. Geotech. Geoenviron.*, **143**(10), p. 06017014 (2017).

39. Badanagki, M., Dashti, S., and Kirkwood, P. "Influence of dense granular columns on the performance of level and gently sloping liquefiable sites", *J. Geotech. Geoenviron.*, **144**(9), p. 04018065 (2018).

40. Bahmanpour, A., Towhata, I., Sakr, M., et al. "The effect of underground columns on the mitigation of liquefaction in shaking table model experiments", *Soil Dyn. Earthq. Eng.*, **116**, pp. 15–30 (2019).

41. Garca-Torres, S. and Madabhushi, G.S.P. "Performance of vertical drains in liquefaction mitigation under structures", *B. Earthq. Eng.*, **17**(11), pp. 5849–5866 (2019).

42. FHWA NHI (Federal Highway Administration-National Highway Institute), *Micro-Pile Design and Construction Reference Manual*, US Department of Transportation, McLean, Va. Publication No. FHWA NHI-05-039 (2005).

43. Komak Panah, A., Jalilian Mashhoud, H., Yin, J.H., et al. "Shaking table investigation of effects of inclination angle on seismic performance of micropiles", *Int. J. Geomech.*, **18**(11), p. 04018142 (2018).

44. Mashhoud, H.J., Yin, J.H., Panah, A.K., et al. "Shaking table test study on dynamic behavior of micropiles in loose sand", *Soil Dyn. Earthq. Eng.*, **110**, pp. 53–69 (2018).

45. Mashhoud, H.J., Yin, J.H., Panah, A.K., et al. "A 1-g shaking table investigation on response of a micropile system to earthquake excitation", *Acta Geotech.*, **15**(4), pp. 827–846 (2020).

46. Capatti, M.C., Dezi, F., Carbonari, S., et al. "Full-scale experimental assessment of the dynamic horizontal behavior of micropiles in alluvial silty soils", *Soil Dyn. Earthq. Eng.*, **113**, pp. 58–74 (2018).

47. El Sharnouby, M.M. and El Naggar, M.H. "Field investigation of lateral monotonic and cyclic performance of reinforced helical pulldown micropiles", *Can. Geotech. J.*, **55**(10), pp. 1405–1420 (2018).

48. Guo, Z., Khidri, M., and Deng, L. "Field loading tests of screw micropiles under axial cyclic and monotonic loads", *Acta Geotech.*, **14**(6), pp. 1843–1856 (2019).

49. Capatti, M.C., Dezi, F., Carbonari, S., et al. "Dynamic performance of a full-scale micropile group: Relevance of nonlinear behaviour of the soil adjacent to micropiles", *Soil Dyn. Earthq. Eng.*, **128**, p. 105858 (2020).

50. McManus, K.J., Charton, G., and Turner, J.P. "Effect of micropiles on seismic shear strain", *GeoSupport 2004: Drilled Shafts, Micropiling, Deep Mixing, Remedial Methods, and Specialty Foundation Systems*, Orlando, Florida, United States, pp. 134–145 (2004).

51. Shahrour, I. and Juran, I. "Seismic behaviour of micropile systems", *Ground Improv.*, **8**, pp. 109–120 (2004).

52. Mitrani, H. and Madabhushi, S.P. "Centrifuge modelling of inclined micro-piles for liquefaction remediation of existing buildings", *Geomech. Geoeng.: An Int. J.*, **3**(4), pp. 245–256 (2008).

53. GuhaRay, A., Mohammed, Y., Harisankar, S., et al. "Effect of micropiles on liquefaction of cohesionless soil using shake table tests", *Innov. Infr. Solut.*, **2**(1), p. 13 (2017).

54. Farhangi, V., Karakouzian, M., and Geertsema, M. "Effect of micropiles on clean sand liquefaction risk based on CPT and SPT", *Appl. Sci.*, **10**(9), p. 3111 (2020).

55. Iai, S. "Similitude for shaking table tests on soil-structure-fluid model in 1g gravitational field", *Soils & Found.*, **29**(1), pp. 105–118 (1989).

56. Iai, S., Tobita, T., and Nakahara, T. "Generalised scaling relations for dynamic centrifuge tests", *Geotechnique*, **55**(5), pp. 355–362 (2005).

57. Vargas-Monge, W. "Ring shear tests on large deformation of sand", Ph.D. Thesis, The University of Tokyo, (1998).

58. JRA (Japan Road Association) "Seismic design specifications for highway bridges", English version, Prepared by Public Works Research Institute (PWRI) and Ministry of Land, Infrastructure and Transport, Tokyo, Japan (2002).

59. Haeri, S.M., Kavand, A., Asefzadeh, A., et al. "Large scale 1-g shake table model test on the response of a stiff pile group to liquefaction induced lateral spreading", *18th International Conference on Soil Mechanics and Geotechnical Engineering*, Paris, pp. 919–922 (2013).

60. Brandenberg, S.J., Wilson, D.W., and Rashid, M.M. "Weighted residual numerical differentiation algorithm applied to experimental bending moment data", *J. Geotech. Geoenviron.*, **136**(6), pp. 854–863 (2010).

Biographies

Ali Kavand has been an Assistant Professor of Geotechnical Engineering at the School of Civil Engineering, College of Engineering, University of Tehran since 2013. He received his PhD degree in Geotechnical Engineering from Sharif University of Technology in 2013 as the first-ranked graduate. His main research interests deal with, but not limited to, experimental and numerical investigations of different geotechnical earthquake engineering problems, especially liquefaction, dynamic characterization of geomaterial, seismic site response analysis, and seismic hazard assessment.

S. Mohsen Haeri, born in 1954 in Tehran, has been a Professor of Civil Engineering, Geotechnical Division, at Civil Engineering Department of Sharif University of Technology, Tehran since 1992. In addition, he has been the Director of Geotechnical Engineering Studies and Research Center (GESRC) of Sharif University of Technology since 2004. He has also served as the Past Chairman of the Civil Engineering Department and Ex-Director of the Earthquake Engineering Research Center at Sharif University of Technology. Professor Haeri was a distinguished MSc graduate in Civil Engineering from University of Tehran, Iran (1976), MSc in Geotechnical Engineering from University of Illinois at Urbana-Champaign, USA (1979), and PhD in Earthquake Geotechnical Engineering from Imperial College, London, UK (1988). His research interest is fairly wide and mainly focuses on the following subjects: static and dynamic soil characterization especially for unsaturated collapsible and cemented gravelly soils; earthquake geotechnical engineering (liquefaction, landslide and local site effects and microzonation); static and dynamic behavior of earth and rockfill dams including cfrd; physical modeling of geotechnical structures, especially study on the effect of liquefaction induced lateral spreading on pile foundations; dynamic soil structure interaction, especially during rocking; deep excavations, mse walls, and retaining structures. Professor Haeri has published 52 refereed Journal Papers and more than 134 conference papers. He has also delivered more than 14 keynote speeches as invited or theme lecturer. He also published 9 books in Farsi. Professor Haeri has taught more than 10 different courses in Geotechnical Engineering and supervised 15 PhD and 94 MSc students in Geotechnical Engineering. Professor Haeri is not only active in the academic fields, but also very active in Scientific and Technical Societies and Committees including ISMGE and IGS. He also made contributions in different Committees of Iranian Code of Practice for Civil Engineers. In addition, he has served as the top Advisor and Head and/or a Member of Panel of Experts for very challenging and large projects such as very high earth dams and arch dams and very deep excavations in difficult grounds.

Javad Raisianzadeh is currently an Assistant Professor at the Department of Civil Engineering, Pardis Branch, Islamic Azad University, Pardis, Iran. He received his PhD degree in Geotechnical Engineering from the School of Civil Engineering, College of Engineering, University of Tehran; MSc degree in Geotechnical Engineering from Sharif University of Technology; and BSc degree in Civil Engineering from Ferdowsi University of Mashhad. His research interests include numerical simulation of the granular media, micromechanics, geotechnical earthquake engineering, and physical modeling.

Sina Afzalsoltani is a PhD candidate at the Sharif University of Technology (SUT) in Tehran, Iran. He received his BSc degree in Civil Engineering from Amirkabir University (Tehran Polytechnic) and MSc degree in Geotechnical Engineering from SUT. He is interested in deep foundations, physical modeling, and thermo-hydro-mechanical behavior of soils.